

arXiv:astro-ph/9807189v1 17 Jul 1998

NEW AND OLD TESTS OF COSMOLOGICAL MODELS AND EVOLUTION OF GALAXIES

Vahé Petrosian

Space Telescope Science Institute, Baltimore, MD 21218

Center for Space Science and Astrophysics, Stanford University, Stanford, CA 94305

Received _____; accepted _____

ABSTRACT

We describe the classical cosmological tests, such as the $\text{Log}N$ - $\text{Log}S$, redshift-magnitude and angular diameter tests, and propose some new tests of the evolution of galaxies and the universe. Most analyses of these tests treat the problem in terms of a luminosity function and its evolution. The main thrust of this paper is to show that this is inadequate and can lead to incorrect conclusions when dealing with high redshift sources. We develop a proper treatment in three parts.

In the first part we describe these tests based on the isophotal values of the quantities such as flux, size or surface brightness. We show the shortcomings of the simple point source approximation based solely on the luminosity function and consideration of the flux limit. We emphasize the multivariate nature of the problem and quantify the effects of other selection biases due to the surface brightness and angular size limitations. In these considerations the surface brightness profile, and the distribution of the basic parameters describing it, play a critical role in modeling of the problem. In general, in the isophotal scheme the data analysis and its comparison with the model predictions is complicated. In the second part we show that considerable simplification is achieved if these tests are carried out in some sort of metric scheme, for example that suggested by Petrosian (1976). This scheme, however, is limited to well resolved sources. Finally, we describe the new tests and compare them to the traditional tests demonstrating the observational and modeling ease that they provide. These new procedures, which can use the data to a fuller extent than the isophotal or metric based tests, amount to simply counting the pixels or adding their intensities as a function of the surface brightness of all galaxies instead of dealing with surface brightnesses, sizes and fluxes (or magnitudes) of individual galaxies. We also show

that the comparison of the data with the theoretical models of the distributions and evolution of galaxies has the simplicity of the metric test and utilizes the data as fully as the isophotal test.

Subject headings: cosmology:theory–galaxies:evolution–galaxies: luminosity function–galaxies:photometry.

1. INTRODUCTION

Galaxies and other extragalactic sources provide the most direct means of studying evolution in the universe. This is done using the classic cosmological tests such as the angular diameter-redshift-magnitude relations or the source counts (also known as the Log N -Log S) test. (For a general description of these tests see, e.g. Weinberg 1972.) These tests, which rely primarily on the distribution of the magnitudes or fluxes of the sources, have had limited success in determining the cosmological parameters and/or the evolution of galaxies. There are two fundamental reasons for this failure. The first is the well-known difficulty of disentangling the evolution of the sources (see e.g. Tinsley 1968 or Tinsley & Gunn 1976) from the evolution of the universe (Weinberg 1972). As a result, over the years, the focus of such studies has been shifted from the determination of the cosmological parameters to the evolution of galaxies in different assumed cosmological models. The second difficulty arises from the fact that galaxies are extended (i.e. resolved) sources and there is ambiguity in defining proper magnitudes (or luminosities L and fluxes l) and diameters. In addition the samples of sources are not merely limited by their fluxes (or magnitudes) but there exist other selection biases or data truncations due to surface brightness or size limitations. These aspects of the problem are usually ignored. This may be an acceptable approximation for high surface brightness sources at low redshifts, but it is woefully inadequate when dealing with data at high redshifts extending to low surface brightness sources. The main purpose of this paper is to present a proper analysis of the various observational biases that are encountered in this process. There are two ways one can carry out this task. From the original data sample one can select a subsample with fewer and simpler biases (as we do in §3), or one may correct the model expectation fully for all known selection biases, which is the approach we take in the rest of the paper. The first method is more appropriate for tests dealing with the moments of the distributions such as

flux-redshift or size-redshift relations. The second method is preferable when dealing with the various source counts and uses all of the valuable data.

The bias due to the magnitude or flux limit is accounted for by various means. The most common practice is to use *isophotal* values, i.e. the values of these quantities up to or at some limiting apparent surface brightness b_{iso} . However, because of the rapid decline of the apparent surface brightness b (defined as flux per unit angular area of a resolved source) with redshift z (see, e.g. Tolman 1934),

$$b = B/(1+z)^4, \quad (1)$$

where B is the intensity or the absolute surface brightness at the source, the biases due to the surface brightness and size limits of the observations become important at high redshifts and/or for low surface brightness sources. These effects are often ignored or are dealt with indirectly by using a limited portion of the available data.

The corrections required for these effects, sometimes referred to as aperture corrections, inevitably require the knowledge of the surface brightness profile

$$B(r) = B_0 f(r/r_0) \quad \text{with} \quad f(0) = 1, \quad (2)$$

and the distributions of the central surface brightness B_0 , the characteristic or core radius r_0 , and other parameters α_i defining the profile $f(x)$. For example, $\alpha = 1$ or $1/4$ for disks or spheroids, respectively, where the profile is described by the simple relation $\ln f(x) = -x^\alpha$. Early examples of methods to correct the redshift magnitude relation for the aperture effect were described by Sandage (1972), using an iterative procedure, and by Gunn & Oak (1975), assuming a fiducial cosmological model. These authors used empirical relations for the luminosity within the radius r ,

$$L(r) = (4\pi)\pi r_0^2 B_0 F(r/r_0) \quad \text{with} \quad F(t) = \int_0^t 2x f(x) dx. \quad (3)$$

It was shown by Petrosian (1976) (P76 hereafter) that these corrections can be carried out more directly. It was also shown in P76 that one can separate the evolution of the surface brightness B_0 from the evolution of universe, and can avoid some of the above difficulties by dealing with the angular sizes and magnitudes up to and within a “proper metric” radius r_p obtained from a specified value of the quantity

$$\eta = \frac{F(x)}{x^2 f(x)} = 2 \frac{d \ln r}{d \ln L(r)} \quad \text{with} \quad x = \frac{r}{r_0}, \quad (4)$$

which is equal to the ratio of the average surface brightness within r to the surface brightness at r .

The above equations describe the source brightness profile and its basic properties in terms of two convenient parameters; the central surface brightness B_0 and core radius r_0 . These parameters are not easily accessible to observations and their relative values for different values of α are difficult to interpret. This difficulty can be overcome if we transfer the above relations to observationally more meaningful parameters. One commonly used such sets of parameters is the effective radius and surface brightness. The effective values refer to the radius containing half the total luminosity L which means $F(r_{\text{eff}}/r_0) = 0.5F(\infty)$. The ratios of the effective to central values are: $B_{\text{eff}}/B_0 = 0.189, 2.54 \times 10^{-2}, 3.45 \times 10^{-3}$ and 4.66×10^{-4} , and $r_{\text{eff}}/r_0 = 1.66, 13.5, 1.82 \times 10^2$ and 3.46×10^3 for $\alpha = 1, 1/2, 1/3$ and $1/4$, respectively.

Figure 1 shows the profile f , the curves of growth of luminosity $F/F(\infty)$ and the function η as a function of $(r/r_{\text{eff}})^\alpha$, for the above values of α . This shows the general and relative characteristics of these functions.

To demonstrate the effects of the redshift, in Figure 2 we show the variation with redshift of the fraction of the luminosity and the area (expressed in magnitude units) within a surface brightness limit b for $\alpha = 1$ and $1/4$ profiles. Instead of the surface brightnesses B_0 and b we use the more familiar magnitudes; $\mu = -2.5 \log b + \text{const.}$, and

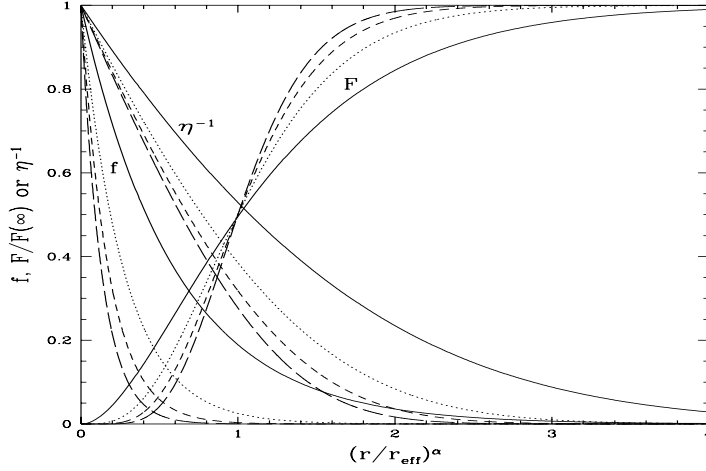


Fig. 1.— Variation of surface brightness profile f , normalized luminosity growth curve $F/F(\infty)$, and the inverse of the η function defined in equation (4) versus $(r/r_{\text{eff}})^\alpha$ for $\alpha = 1, 1/2, 1/3$, and $1/4$ (solid, dotted, short dashed, and long dashed lines, respectively). Note that $\ln f = -(r/r_{\text{eff}})^\alpha (r_{\text{eff}}/r_0)^\alpha$ and the effective radius r_{eff} is defined as $F(r/r_{\text{eff}}) = 0.5F(\infty)$.

$\mu_{\text{eff}} = -2.5\log(B_{\text{eff}}) + \text{const.}$. As evident the observable area and luminosity vary rapidly with redshift, specially for low surface brightnesses and have a different behavior for the two profiles. This will produce a variation with redshift of the relative abundances of disks and spheroids. Another possible representation of the above graphs will be in terms of the proper metric radius r_p defined above. This is preferable because this definition of radius relies on the data within some measured isophot and not on the unobserved outer parts which are needed to determine the effective radius r_{eff} . This procedure will be developed further in §3.

In this paper we review several old procedures and propose some new ones for the study of the evolution of galaxies, and possibly that of the universe, whereby instead of dealing with individual galaxies we deal with the combined brightness of all galaxies. The new methods simplify the data analysis enormously and are perfectly suited for modern digitized

data. In §2 we first give a brief description of the proper analysis of the classical tests for isophotal quantities that includes all the observational selection effects as well as the effects of the surface brightness profile, and treats the problem in terms of the multivariate distribution $\psi(B_0, r_0, \alpha_i, z)$ instead of the commonly used luminosity function $\phi(L, z)$.

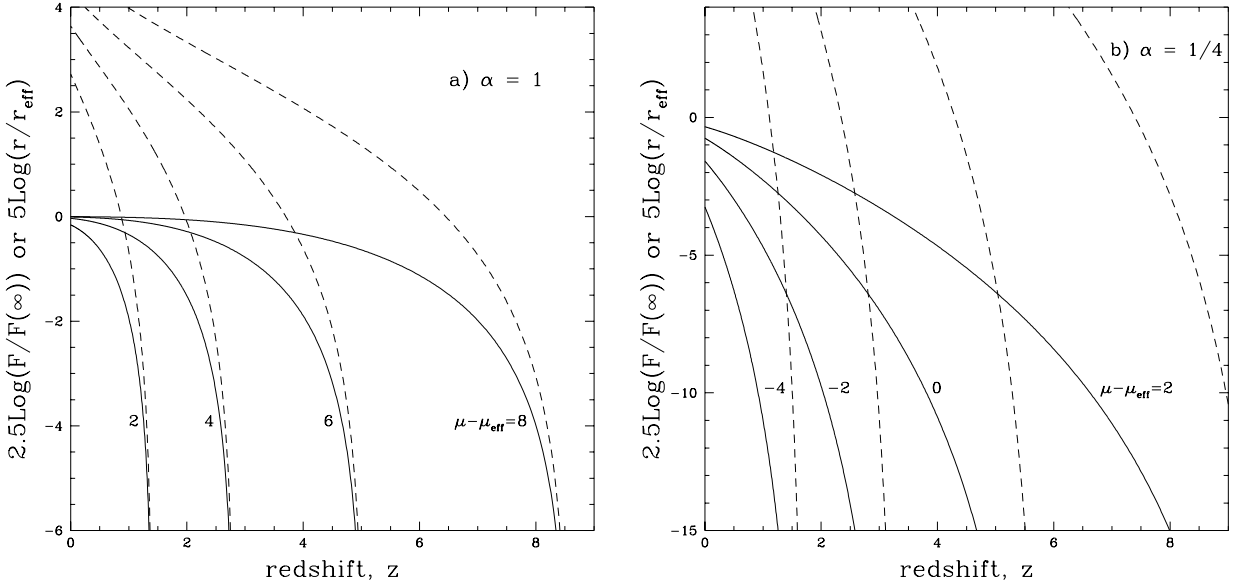


Fig. 2.— Variation of the fraction of the luminosity (solid lines) and projected surface area (dashed lines), in some arbitrary magnitude units, within a surface brightness isophot μ versus redshift for several values of the effective surface brightness μ_{eff} . a) for an exponential (disk) profile, $\ln f = -x$; b) for a de Vaucouleurs profile, $\ln f = -x^{1/4}$. Note that for each value of μ_{eff} the luminosity and area shrink rapidly as we approach the maximum redshift $z_{\text{max}} = (B_0/b)^{1/4} - 1$, where B_0 and b are related to μ_{eff} and μ as described in the text. Also note that this decline is more pronounced for disks than spheroids indicating that the relative populations of sources with different profiles will vary strongly with redshift.

There are several reasons for the popularity of the latter procedure. The first is that we have accumulated a considerable knowledge about the local luminosity function of galaxies (see e.g. Efstathiou et al. 1988 and Lin et al. 1966) but little information on

the distributions of the B_0 and r_0 (see, e.g. Sandage & Perelmuter, 1991). Secondly, until recently it was believed that the distribution of the surface brightness was fairly narrow (Fish, 1964; Freeman, 1970). However, in recent years, because of increasing interest in low surface brightness dwarf galaxies, some data has been accumulated on the intrinsic distributions of these parameters indicating broad distributions (see e.g. McGaugh 1996; de Jong 1996; Tully & Verheijen 1997; Impey & Bothun 1997 and references cited there). Of course, one can use the luminosity function by replacing the total luminosity $L = (4\pi)\pi r_0^2 B_0 F(\infty)$ [see eq. (3)] for either B_0 or r_0 . In any case a multivariate description is required. In §3 we repeat the analysis of §2 for metric quantities. In §4 we describe the new tests and their relations to the multivariate distribution ψ and the profile $f(r)$. Finally, in §5 we give a brief summary.

2. CLASSICAL TESTS: ISOPHOTAL VALUES

The classical test use the observed relations between the magnitude (or flux l), angular size (radius θ or area $\pi\theta^2$) and redshift to determine the cosmological parameters and the evolution of sources as described by the general “luminosity” function ψ . The cosmology is introduced via the relations

$$l(\theta) = (4\pi)\pi r_0^2 B_0 F(r) / (4\pi d_L^2(z, \Omega_i)) \quad \text{and} \quad \theta = r/d_A(z, \Omega_i), \quad (5)$$

where d_L and $d_A = d_L/(1+z)^2$ are the luminosity and the angular diameter distances, and Ω_i represent the cosmological parameters such as the density parameter Ω , the deceleration parameter q_0 or the cosmological constant Λ (see, e.g. Weinberg 1972). All the classical tests can be described in terms of the observed distribution of flux, size and redshift; $n(l, \theta, z)$. For the purpose of the demonstration of the effects that we would like to emphasize here, let us consider the cumulative source counts as a function of redshift, which we denote by

$N(> l, > \theta, z)$. The cumulative and differential counts of the so called Log N -Log S relation is obtained by the integration of the above expressions over the redshift.

For simplicity, in the above relation and in what follows, we ignore cosmological attenuation, if any, assume either bolometric (or monochromatic) fluxes, so that we can ignore the K-correction, and assume spherical symmetry with brightness profile $f(r)$ independent of the wavelength. The complications due to K-correction, asphericity, etc. can be easily included in the relations that follow. We will address some aspects of these in §5.

2.1. Point Sources

The usual practice (see, e.g. Metcalfe et al. 1995 or Tyson, 1988) is to compare the observed cumulative and differential distributions $N(> l, z)$ and $n(l, z) = -\partial N(> l, z)/\partial l$ (and their integrals over redshift) with that expected from models via the relations

$$N(> l, z) = \frac{dV}{dz} \int_{4\pi d_L^2 l}^{\infty} \phi(L, z) dL \quad \text{and} \quad n(l, z) = \frac{dV}{dz} 4\pi d_L^2 \phi(4\pi d_L^2 l, z), \quad (6)$$

where $V(z, \Omega_i)$ is the co-moving volume up to redshift z and $\rho(z) = \int_0^{\infty} \phi dL$ is the co-moving density of all sources at z . Here and in what follows we assume a complete 4π steradian sky coverage. These expressions is what one would expect for unresolved or point sources, where only the flux limit counts in the selection process (see, however, a modification below in §2.3).

2.2. Extended Sources

For extended sources such as galaxies the selection process is more complex and additional corrections are required. We now describe these selection biases.

2.2.1. Surface Brightness Limit

A source to be detected must have an apparent central surface brightness exceeding the detection threshold which must be several times the standard deviation σ of the fluctuations in the background brightness. We denote this limit by b_{iso} . If we ignore the image degradation due to the finite size of the instrumental and atmospheric point spread function (PSF), which can be done if the core size $r_0 \gg \theta_s d_A$, and if the pixel size is less than or comparable to the width θ_s of the PSF, then the surface brightness selection criterion requires that

$$B_0 \geq B_{\text{iso}} \equiv (1+z)^4 b_{\text{iso}}. \quad (7)$$

However, for small sources or high redshifts the effect of the finite size of the PSF cannot be ignored and the selection bias is more severe than indicated by this relation. For a PSF = $g(\theta/\theta_s)$ the surface brightness is modified to

$$\hat{B}(r) = \hat{B}_0 \hat{f}(r/r_0, \theta_s d_A/r_0), \quad \text{where } \hat{f} = f * g \quad (8)$$

is the convolution of the the actual profile with the PSF. As a result, the central surface brightness is reduced by $\xi = \hat{B}_0/B_0$, where

$$\xi(\theta_s d_A/r_0) = \int_0^\infty f(\theta d_A/r_0) g(\theta/\theta_s) \theta d\theta / \int_0^\infty g(\theta/\theta_s) \theta d\theta. \quad (9)$$

For the purpose of illustration let us consider a box PSF with the radial width of θ_s . This reduction factor then simplifies and equation (7) is modified to read

$$B_0 \geq B_{\text{iso}} x_s^2 / F(x_s) \quad \text{with } x_s = \theta_s d_A / r_0. \quad (10)$$

Similar expressions can be derived for other forms of the PSF. For $x_s \ll 1$ this reduces to equation (7) but its effects become important for x_s near unity i.e. for partially resolved and unresolved sources. Note that θ_s is replaced by the pixel size θ_{pix} if $\theta_s < \theta_{\text{pix}}$

2.2.2. Size Limit

Another criterion for selection of extended sources such as galaxies is that their sizes must exceed some limit. One way to quantify this is to have the isophotal angular radius (namely, the radius where the surface brightness has dropped to the specified isophotal value b_{iso}) be larger than some specified size θ . If $\theta \gg \theta_s$, then the isophotal angular radius is given by

$$\theta_{\text{iso}} = (r_0/d_A)f^{-1}(B_{\text{iso}}/B_0), \quad (11)$$

where the function f^{-1} is the inverse of the profile function f . Then the selection condition $\theta_{\text{iso}} \geq \theta$ is satisfied if

$$B_0 \geq B_{\text{iso}}/f(\theta d_A/r_0). \quad (12)$$

However, as θ decreases toward θ_s one should use the modified profile \hat{f} of equation (8) in place of f . In any case, it is clear that for $\theta \geq \theta_s$ this inequality will provide a more restrictive limit than the surface brightness limit because it requires that more than one pixel to exceed the surface brightness limit b_{iso} . This can be demonstrated mathematically also by setting $\theta = \theta_s$ in the last equation and comparing it with the limit in equation (10). The ratio of the two limits is equal to $\eta(x_s)$ which according to equation (4) is greater than one, except for the unlikely event of the surface brightness increasing with r . In the opposite case when $\theta < \theta_s$ one is dealing with unresolved or point like sources in which case a size limit does not make sense.

For non-spherical sources we can follow a similar procedure by dealing with the isophotal angular area ω (which for spherical sources is equal to $\pi\theta^2$) as the area of the sources with apparent surface brightness $b \geq b_{\text{iso}}$. However, the relation of this to the surface brightness profile will be more complicated. For example, for elliptical sources with a constant ellipticity we can express the profile f as a function of the area a/a_0 with $a_0 = \pi r_1 r_2$, where r_1 and r_2 are the core radii along the major and minor axes. For randomly oriented

elliptical sources this will amount to replacement of the quantity $\theta d_A/r_0$ in equation (12) by $(\omega d_A^2/a_0)^{1/2}$. The distribution function ψ now will be a function of a_0 and the ellipticity or the ratio r_1/r_2 .

2.2.3. Flux Limit

Finally the sample of sources is subject to a flux limit. In this section we consider the flux l_{iso} within the isophotal angular radius θ_{iso} or up to the surface brightness limit b_{iso} . The flux limit then implies that $l_{\text{iso}} = L(\theta_{\text{iso}} d_A)/4\pi d_L^2$ is greater than some specified flux l . Using equations (3) and (5) we can write this limit as

$$B_0 F(x_{\text{iso}}) \geq d_L^2 l / (\pi r_0^2) \quad \text{with} \quad x_{\text{iso}} \equiv \theta_{\text{iso}} d_A / r_0 = f^{-1}(B_{\text{iso}}/B_0). \quad (13)$$

Note that the left hand side of this inequality is independent of r_0 . However, if $\theta_{\text{iso}} \gg \theta_s$, then one should replace the profiles f and its integral the luminosity growth curve F by the corresponding values, \hat{f} and \hat{F} , modified by the PSF. In this case the above relation becomes more complex with the involvement of the additional variable $\theta_s d_A / r_0$ (see §2.4 below).

2.2.4. Combined Limits

Thus, for a given value of $\theta, l, b_{\text{iso}}$ and θ_s the above three inequalities determine the region of the $B_0 - r_0$ plane that is accessible at these particular conditions. This region varies with redshift becoming smaller at higher redshifts. The redshift dependences are hidden in B_{iso} and d_A . Figure 3 show the three boundary conditions obtained by the equality sign in equations (10), (12) and (13) for the exponential, $\alpha = 1$, and de Vaucouleurs, $\alpha = 1/4$, profiles. We plot B_0/B_{iso} versus $r_0/(\theta_s d_A)$, which is valid at all redshifts. The lowest

(heavy) solid line shows the truncation due to the surface brightness limit. The lighter solid lines show the effects of the size limit for several values of θ/θ_s . The dashed lines show the truncation due to the flux limit for different values of the ratio $l/(\pi\theta_s^2 b_{\text{iso}})$. Sources lying in the region above all three lines are the ones which satisfy all the selection criteria. It is clear that, as long as $\theta > \theta_s$, or $l > \pi\theta_s^2 b_{\text{iso}}$, which obviously will be the case for resolved sources, the surface brightness limit due to the PSF, described by equation (10), is never important. However, both size and flux limits could be important depending on the relative values of the observational limits. For larger values of the ratio $l/(\pi\theta_s^2 b_{\text{iso}})$ the flux limit provides the major constraint. In the opposite case the size limit becomes more important, and as evident from the above figures for $l = \pi\theta_s^2 b_{\text{iso}}$ only the size limit is relevant.

2.2.5. Extended Source Counts

We can now relate the observable $N(>l, >\theta, z)$ to the distribution function $\psi(B_0, r_0, z)$ by the integration of the latter over the accessible region as determined by the observational limits. For the general case this gives

$$N(>l, >\theta, z) = \frac{dV}{dz} \left(\int_{B_{\text{iso}}}^{B_{0,cr}} dB_0 \int_{r_{0,1}}^{\infty} dr_0 \psi(B_0, r_0, z) + \int_{B_{0,cr}}^{\infty} dB_0 \int_{r_{0,2}}^{\infty} dr_0 \psi(B_0, r_0, z) \right). \quad (14)$$

Here $r_{0,1}$ and $r_{0,2}$ are obtained by solving equations (13) and (12) for r_0 in terms of B_0 and other observables, and

$$B_{0,cr} = B_{\text{iso}} / f \left(\eta^{-1} \left(l / (\pi\theta_s^2 b_{\text{iso}}) \right) \right), \quad (15)$$

is the intersection point of the the two boundary conditions described by equations (12) and (13) or the intersection of a solid and a dashed line in Figure 3; η^{-1} is the inverse function of the function η defined in equation (4). Note that as stated above for $l = \pi\theta_s^2 b_{\text{iso}}$ this critical value of surface brightness becomes equal to B_{iso} , the first double integral in

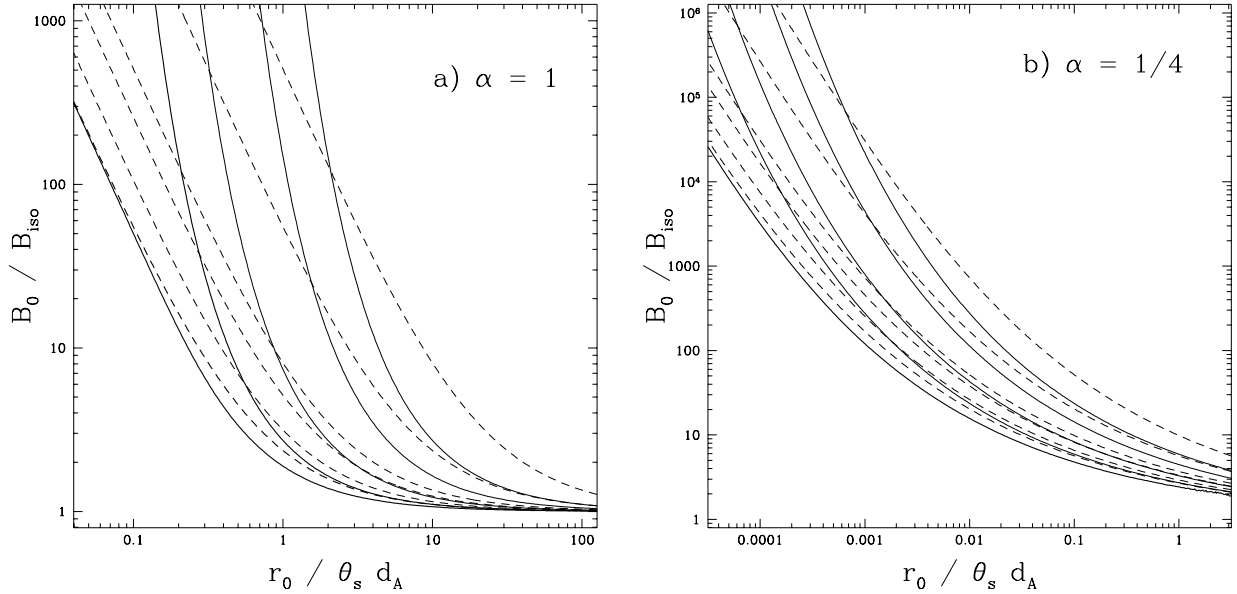


Fig. 3.— Central surface brightness B_0 in units of $B_{\text{iso}} = b_{\text{iso}}(1 + z)^4$ versus the size r_0 in units of $\theta_s d_A$ depicting the surface brightness limit (the heavy or lowest solid line); the angular size limit for $\theta/\theta_s = 1, 2, 5$ and 10 (thin solid lines); and the flux limit for $l/\pi\theta_s^2 b_{\text{iso}} = 1, 2, 5, 10, 100$ and 1000 (dashed lines). a) for an exponential (disk) profile, $\ln f = -x$; b) for a de Vaucouleurs profile, $\ln f = -x^{1/4}$. Note that the solid and dashed lines cross each other where the limiting factor changes from size to flux. The region to the right of the appropriate solid line before these intersections and to the right of the appropriate dashed line after the intersections are accessible to observation. Note also that, because B_{iso} and d_A increase with redshifts, the observable region shrinks systematically, moving towards the upper right hand corner, as redshift increases.

the left hand side of equation (14) vanishes and we are left with the size limited part of this expression only.

It is clear, therefore, that the relation for the counts of extended sources is considerably more complicated than the commonly used relation (6). In order to see these differences more clearly we can rewrite the above expressions in terms of the luminosity L . For example, if we replace r_0 by $L = (4\pi)\pi r_0^2 B_0 F(\infty)$ we can rewrite all the boundary conditions in terms of B_0 and L instead of B_0 and r_0 . The three limits in equations (10), (12) and (13) now give, respectively, the conditions

$$B_0 \geq B_{\text{iso}} \left(F^{-1}(\lambda) \right)^2 / \lambda, \quad \text{with } \lambda = 4\pi d_L^2 (\pi \theta_s^2 b_{\text{iso}}) F(\infty) / L, \quad (16)$$

$$L \geq L_{\min, \theta} \equiv 4\pi d_L^2 (\pi \theta_s^2 b_{\text{iso}}) F(\infty) / \left(x_{\text{iso}}^2 f(x_{\text{iso}}) \right), \quad (17)$$

and

$$L \geq L_{\min, l} \equiv 4\pi d_L^2 l F(\infty) / F(x_{\text{iso}}). \quad (18)$$

Here F^{-1} is the inverse function of the luminosity curve of growth F and x_{iso} is a function of B_0 / B_{iso} (eq. [13]). Figure 4 shows the truncations produced by the above selection criteria in the $B_0 - L$ plane.

If we define the distribution $\bar{\psi}(B_0, L, z) = \psi(B_0, L, z) dr_0 / dL$, equation (14) then becomes

$$N(> l, > \theta, z) = \frac{dV}{dz} \left(\int_{B_{\text{iso}}}^{B_{0,cr}} dB_0 \int_{L_{\min, l}}^{\infty} dL \bar{\psi}(B_0, L, z) + \int_{B_{0,cr}}^{\infty} dB_0 \int_{L_{\min, \theta}}^{\infty} dL \bar{\psi}(B_0, L, z) \right). \quad (19)$$

So far we have expressed our results in terms of the central surface brightness B_0 and core radius r_0 . As mentioned in §1 these parameters are not convenient for comparing the results with observations. This task can be carried out more readily if we express the above relations in terms of observationally more meaningful parameters such as the effective radius and surface brightness defined in §1. In Figure 5 we show the size and flux limits

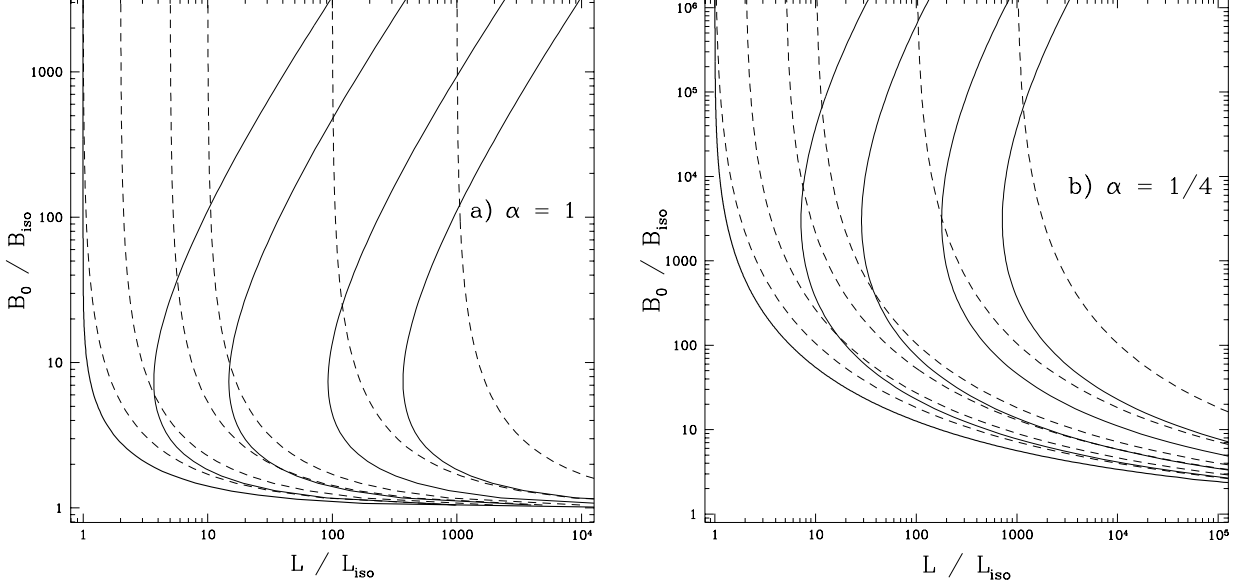


Fig. 4.— Same as Fig. 3 except for the $B_0 - L$ plane. The curves are plotted for the same limiting values as in Fig. 3. The luminosity unit $L_{\text{iso}} = 4\pi d_L^2(\pi\theta_s^2 b_{\text{iso}})$.

in the surface brightness-luminosity plane for both profiles, where instead of the surface brightnesses b_{iso} and B_0 we use the more familiar magnitudes; $\mu_{\text{iso}} = -2.5\text{Log}b_{\text{iso}} + \text{const.}$, and $\mu_{\text{eff},z} = -2.5\text{Log}B_{\text{eff}} + 10\text{Log}(1+z) + \text{const.}$. This figure demonstrates that the region of $B_0 - L$ plane accessible to observations is different for the two profiles and shrinks with increasing redshift.

2.2.6. Comparison With The Point Source Approximation

There are several ways that this correct description differs from the approximate expression given by equation (6). Some of these were discussed by Yoshii (1993). The first difference is the existence of the second set of integrals in equations (14) and (19) which we discussed above. Even at high values of the flux limit, $l \gg \pi\theta^2 b_{\text{iso}}$, when this additional term is negligible there are two other important differences. The first is due to the presence

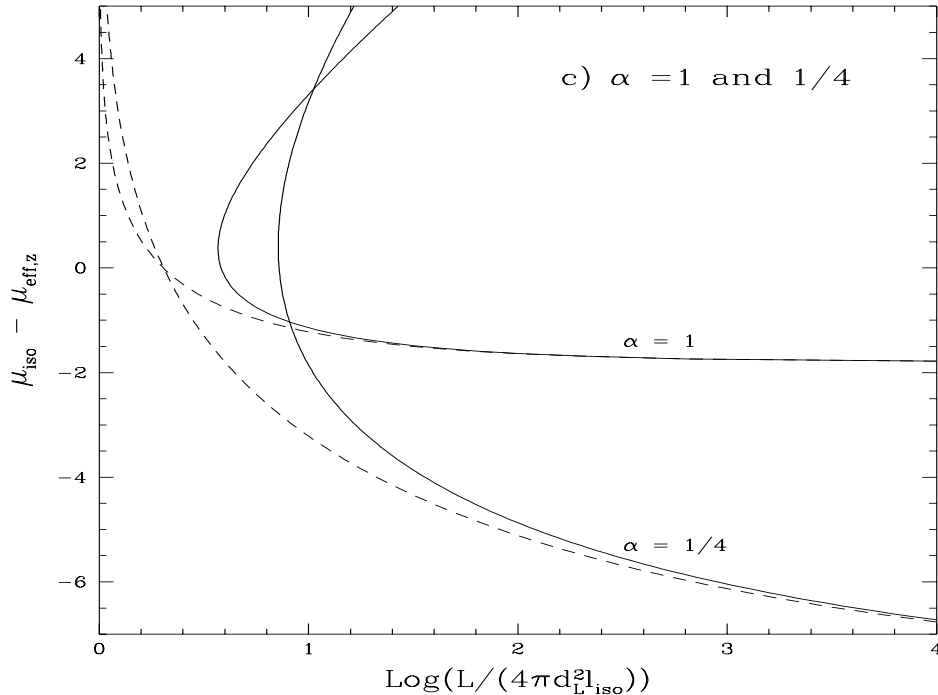


Fig. 5.— Same as Fig. 4 except we plot the combined size and flux limits in terms of the *effective* values of the surface brightness in magnitudes; $\mu_{\text{iso}} = -2.5\text{Log}(b_{\text{iso}}) + \text{const.}$ and $\mu_{\text{eff},z} = -2.5\text{Log}(B_{\text{eff}}) + 10\text{Log}(1+z) + \text{const.}$. For clarity, only curves for $\theta = \theta_s$ and $l = \pi\theta_s^2 b_{\text{iso}}$ are shown.

of the ratio $F(\infty)/F(x_{\text{iso}})$ in the lower limit of the luminosity $L_{\min,l}$, which is absent from the lower limit in equation (6). The second effect is due to the breadth of the distribution of B_0 . For narrower distributions this effect is smaller and disappears for a delta function distribution of B_0 .

These differences can be seen in Figures 4a and 4b as follows. For a given value of l or the ratio $l/\pi\theta_s^2 b_{\text{iso}}$ the point source approximation given by equation (6) truncates the $B_0 - L$ plane by a vertical line at the asymptote of dashed line appropriate for this ratio. Then counts all the sources to the right of this line ($L \geq 4\pi d_L^2 l$), irrespective of their surface brightness B_0 , and uses $\phi(L, z) = \int_0^\infty \bar{\psi}(B_0, L, z) dB_0$. Equation (19), on the other hand, indicates that this is an overestimation of the counts and that we should count only sources which lie to the right of both a solid and a dashed lines appropriate for the ratios θ/θ_s and $l/\pi\theta_s^2 b_{\text{iso}}$, respectively. It is, therefore, clear that ignoring the surface brightness and size limitations can cause significant errors the extent of which can be quantified only if we know the distribution function $\bar{\psi}$. We have a good knowledge of the dependence of $\bar{\psi}$ on L at low z and high B_0 but we have only scanty information on its form at high z and low values of B_0 . The primary aim of the cosmological tests under the discussion here is to determine the variation with redshift of the general distribution function $\bar{\psi}$. A detailed investigation of these aspects are beyond the scope of this paper. Here we make some simple comparisons between the extended and point source results which do not require a knowledge of the distribution of B_0 .

1) *Luminosity limits.* The ratio of the limiting luminosities $L_{\min,l}$ and/or $L_{\min,\theta}$ to the limit $4\pi d_L^2 l$ of the point source approximation, which depends only on the surface profile, are shown in Figure 6, for $\alpha = 1$ and $1/4$, respectively, and for several values of the surface brightness (actually the ratio B_0/B_{iso}) and the ratio $\varrho = l/(\pi\theta_s^2 b_{\text{iso}})$. We use the effective rather the central surface brightness and express the above ratios in magnitudes. As evident for high values of the ratio ϱ , i.e. for higher flux limits, there is an increasing bias against

detection of extended sources at higher redshifts. At lower values of this ratio there is additional bias against detection of galaxies at low redshifts due to the size limit.

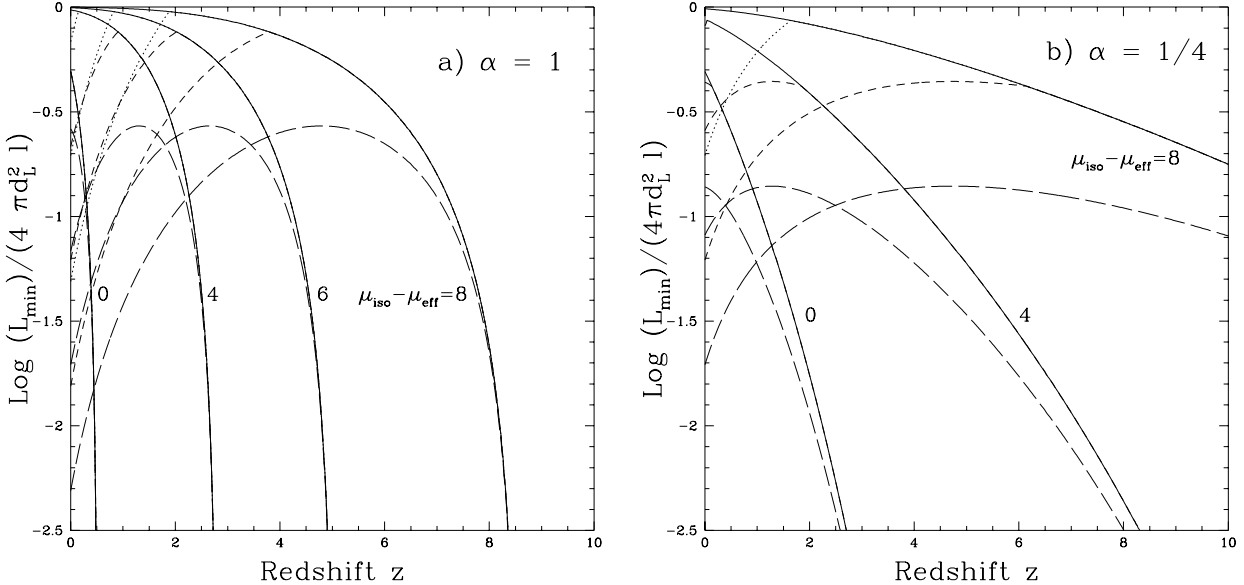


Fig. 6.— The ratio of the minimum detectable luminosity for extended sources in the isophotal scheme [eqs. (17) and (18)] to that of point sources versus redshift, for indicated values of the effective surface brightnesses (more exactly the ratio B_0/b_{iso}) and for four values of the ratio $\varrho = l/(\pi\theta^2 b_{\text{iso}}) = 1, 3.16, 10$ and ∞ , represented by long dashed, short dashed, dotted and solid lines, respectively. a) for an exponential (disk) profile, $\ln f = -x$; b) for a de Vaucouleurs profile $\ln f = -x^{1/4}$. Note the rapid suppression of the flux, as in Fig. 2, when we approach the maximum redshift $z_{\text{max}} = (B_0/b_{\text{iso}})^{1/4} - 1$, where the relation of B_0 and b_{iso} with μ_{eff} and μ_{iso} , respectively, are described in the text. Note also the differences between disks and spheroids as in Fig. 2.

2) *Redshift Distributions.* These differences can also be seen when we compare the redshift distributions expected for point and extended sources. For the purpose of illustration let us assume that L and B_0 are uncorrelated (clearly not a good assumption) so that we can separate the distribution function as $\bar{\psi} = \rho(z)h(B_0)\phi(L/L^*)/L^*$, where $\rho(z)$

and $L^*(z)$ describe the density and luminosity evolution of the sources, and $h(B_0)$ gives the distributions of the central surface brightness. If we define the cumulative functions $H(B_0) = \int_0^\infty h(B_0)dB_0$ and $\Phi(x) = \int_x^\infty \phi(x')dx'$, with $H(0) = \Phi(0) = 1$, then equations (6) and (19) become, respectively

$$N(>l, z) = \frac{dV}{dz} \rho(z) \Phi(4\pi d_L^2 l / L^*) \quad (20)$$

and

$$N(>l, >\theta, z) = \frac{dV}{dz} \rho(z) \left(\int_{B_{\text{iso}}}^{B_{0,cr}} h(B_0) \Phi(L_{\min,l}/L^*) dB_0 + \int_{B_{0,cr}}^\infty h(B_0) \Phi(L_{\min,\theta}/L^*) dB_0 \right). \quad (21)$$

In absence of an exact knowledge of the distribution $h(B_0)$, we compare these expressions for different assumed values of the central or effective surface brightness which amounts to a delta function approximation of $h(B_0)$. In this case equation (21) simplifies to

$$N(>l, >\theta, z) = \frac{dV}{dz} \rho(z) \begin{cases} \Phi(L_{\min,l}/L^*), & \text{if } B_{0,cr} > B_0; \\ \Phi(L_{\min,\theta}/L^*), & \text{if } B_{0,cr} < B_0. \end{cases} \quad (22)$$

Assuming a Schechter luminosity function, $\phi(x) \propto x^p e^{-x}$, we evaluate the redshift distributions for some representative values of the surface brightness B_0 (or μ_{eff}) and for several combinations of the limits l (or magnitude m), θ and b_{iso} (or μ_{iso}). The results are shown in Figure 7 for $p = -1$, and for a cosmological model with $\Omega = 1$ and $\Lambda = 0$. We also assume absence of any density or luminosity evolutions; ρ and L^* constants.

It should be noted that the relative shapes of the point source and various extended source distributions are independent of the cosmological model or the density evolution $\rho(z)$. As evident equation (6) or (20) give quite incorrect redshift dependences, overestimating the number of sources by a large factor at high redshifts, specially for low values of the surface brightness due to the surface brightness limit, and at high values of surface brightness due to the size limit. Clearly ignoring these effects could lead to incorrect results. For example, if these expressions were used to derive the extent of the luminosity evolution, $L^*(z)$, they

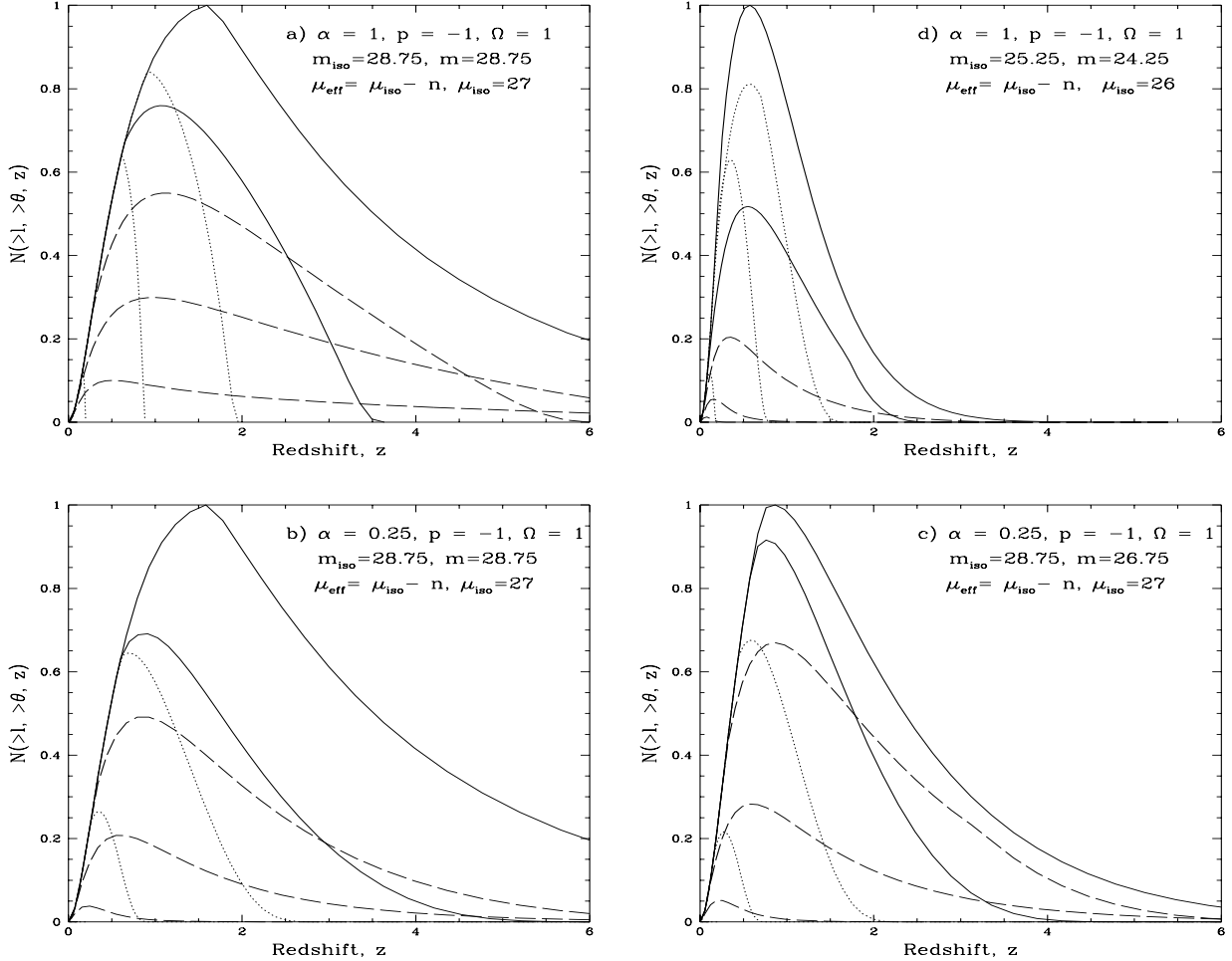


Fig. 7.— The redshift distribution $N(> l, z)$ of equation(20) of the point sources (top heavy solid lines) and extended sources, equation (22), for seven different values of the effective surface brightness. All curves are normalized by the peak value of the point source distribution. In each case the dotted lines are for low surface brightnesses ($n = -1, 1$ and 3) falling below the turning point of the solid lines in Fig. 4c, where the surface brightness limit is most important, and the dashed lines are for high surface brightnesses ($n = 7, 9$ and 11) above this turning point, where the size limit is important. The thin solid line (with $n = 5$) lies generally near the turning point. The limiting magnitude is $m = 2.5\log l + \text{const}$ and $m_{\text{iso}} = -2.5\log(\pi\theta_s^2 b_{\text{iso}}) + \text{const.}$ The surface brightness is in units of magnitude per square arcsec. *a* and *d* for disks, and *b* and *c* for spheroids with different limits.

would underestimate this evolution by factors equal to $F(x_{\text{iso}})/F(\infty)$ and $x_{\text{iso}}^2 f(x_{\text{iso}})/F(\infty)$, depending whether $l/(\pi\theta^2 b_{\text{iso}}) \gg 1$ or is equal to 1, respectively. The situation is more complicated when the effects of the dispersion of the surface brightness or its correlation with the luminosity (or core size r_0) are included. In such cases there would be errors in the determination of the density evolution as well.

3) *Source Counts.* Integrating the redshift distributions over z gives the cumulative counts. Differentiation of this gives the differential counts. For example, for point sources $n(l) = \int_0^\infty \frac{dV}{dz} \phi(4\pi d_L^2 l, z) (4\pi d_L^2) dz$. Figure 8 shows the differential magnitude counts of extended sources with various values of surface brightness as well as that of point sources. We use the same model parameters as above. Again, as evident the neglect of the selection aspect discussed above can cause considerable error in the determination of the evolution of the general luminosity function or the cosmological parameters.

2.3. Point Sources Revisited

It should be noted that some of these effects are present even for unresolved or point sources. However, in this case the correct equation is only slightly different than equation (6) or (20). When $\theta_s d_A \gg r_{\text{eff}}$ the sources are unresolved and they all have essentially the same profile g and size θ_s as the PSF; $\hat{B}(\theta) = B_0 \xi(\theta_s d_A / r_0) g(\theta / \theta_s)$. The total luminosity can be written as $L = 4\pi d_A^2 (\pi \theta_s^2) B_0 \xi$. If we limit ourselves to the isophotal fluxes $> l$ and sizes $> \theta$, then the three selection criteria (eqs. [10], [12] and [13]) become almost identical in form; $B_0 \geq B_{\text{iso}} / (K_i \xi(\theta_s d_A / r_0))$, where ξ is defined in equation (9) and $K_i = 1, g(\theta / \theta_s)$ and $(4\pi)(\pi \theta_s^2 b_{\text{iso}}) G(\theta_{\text{iso}} / \theta_s) / l$, respectively for the three limits. In the above relations we have defined the cumulative PSF as $G(x) = \int_0^x 2g(x) dx$, $G(\infty) = 1$, and θ_{iso} is obtained from $g(\theta_{\text{iso}} / \theta_s) = B_{\text{iso}} / (B_0 \xi) = L_{\text{iso}} / L$. Clearly the size limit does not make sense for unresolved sources and the flux limit is the most restrictive limit. It can be shown then

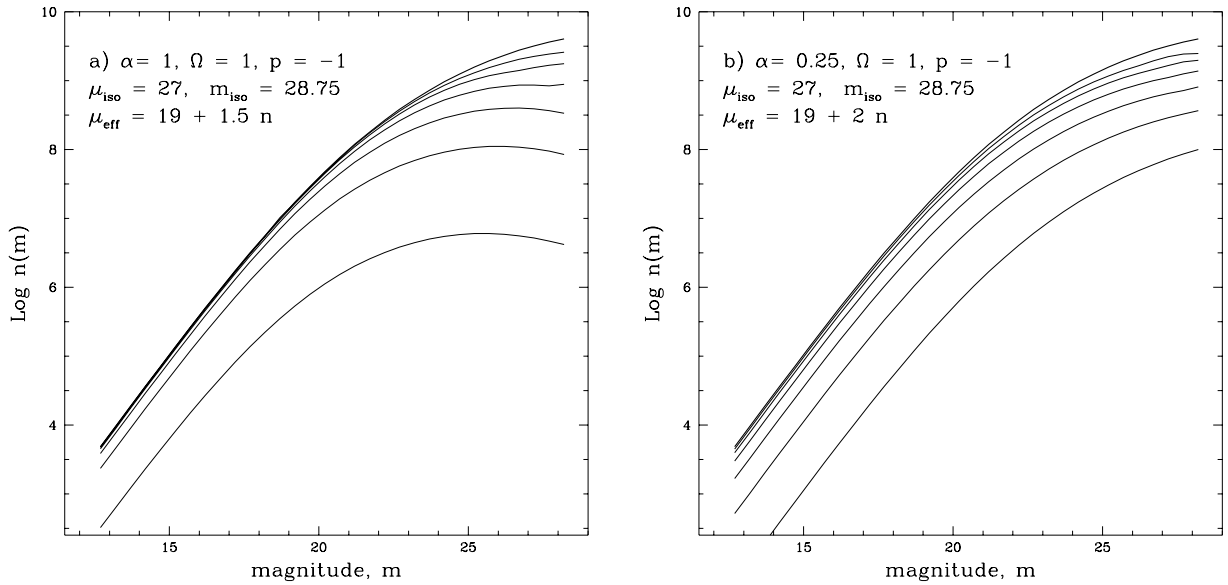


Fig. 8.— The differential counts of point sources (top thick line) and that of extended sources with different surface brightness limits (thin lines with $n = 1$ to 6 from top to bottom) for the same model parameters as Fig. 7. a) for an exponential (disk) profile, $\ln f = -x$; b) for a de Vaucouleurs profile $\ln f = -x^{1/4}$. Note the reduction at large magnitudes for high surface brightness sources and large suppression at all magnitudes for low surface brightness sources.

that the correct expression for the source counts is

$$N(>l, z) = \frac{dV}{dz} \int_{B_{\text{iso}}}^{\infty} dB_0 \int_{L_{\min},s}^{\infty} dL \bar{\psi}(B_0, L, z), \quad (23)$$

where the lower limit of the luminosity is obtained from the solution of

$$LG \left(g^{-1}(L_{\text{iso}}/L) \right) = 4\pi d_L^2 l, \quad \text{with} \quad L_{\text{iso}} \equiv 4\pi d_L^2 (\pi \theta_s^2 b_{\text{iso}}). \quad (24)$$

Here g^{-1} is the inverse function of the PSF. In addition to the surface brightness cutoff and the integration over B_0 , this expression differs from the simple equation (6) also by the presence of the term involving the cumulative PSF G in the integration limit. This difference becomes important only for flux limits very near the isophotal values; $l = \pi \theta_s^2 b_{\text{iso}}$. The surface brightness limit can be important for unresolved galaxies because of their low intrinsic surface brightness or effective temperatures. But for other point sources such as quasars whose surface brightness is equal to that of a hot accretion disk this effect is negligible (becoming important only at extremely high redshifts) and the point source approximation of equation (6) is very accurate.

2.4. Combined Counts

In principle we can combine the counts of the resolved and unresolved sources by replacement of the $B(r)$ with the modified profile $\hat{B}(r)$ of equation (8). We can then repeat the procedure carried out for the extended sources with the replacement of the profiles f and F with \hat{f} and \hat{F} and change the limits correspondingly, except now the profiles are functions of the additional parameter $\theta_s d_A / r_0$. However, now the size limit is unnecessary because we can include all sources. Of course one must make sure that the sample of galaxies, for example, is not contaminated by other unresolved sources (e. g. stars). We therefore have the simpler expression

$$N(>l, z) = \frac{dV}{dz} \int_{B_{\text{iso}}}^{\infty} dB_0 \int_{\hat{L}_{\min},l}^{\infty} dL \bar{\psi}(B_0, L, z), \quad (25)$$

where $\hat{L}_{\min,l}$ is given by equation (18) with $F(x_{\text{iso}}) \rightarrow \hat{F}(x_{\text{iso}})$; note that $\hat{F}(\infty) = F(\infty)$. The parameter x_{iso} now is obtained from $\hat{f}(x_{\text{iso}}, \theta_s d_A / r_0) = B_{\text{iso}} / \hat{B}_0$ with $\pi r_0^2 = L / (4\pi B_0 F(\infty))$.

2.5. Other Tests

Differentiation of $N(>l, >\theta, z)$ gives the differential distribution $n(l, \theta, z)$ from which we can calculate various moments and compare them to observations. For example, the flux-redshift relation can be obtained from

$$\langle l(z) \rangle = \int_l^\infty \left(L F(x_{\text{iso}}) / (4\pi d_L^2 F(\infty)) \right) n(l, >\theta, z) dl / N(>l, >\theta, z). \quad (26)$$

In a similar fashion one can derive $\langle \theta \rangle - z$ or $\langle \theta \rangle - \langle l \rangle$ relations.

3. CLASSICAL TESTS: METRIC VALUES

Some of the complications evident in the above analysis can be avoided if instead of the isophotal sizes and fluxes we deal with some metric values of these quantities. For example, if we define a proper metric size r_p corresponding to a constant value of the function η , say η_0 , as defined in P76 and equation (4), then the expressions for the surface brightness, size and flux limits (or truncations) become considerably simplified. For a limiting surface brightness b_{iso} , a limiting angular radius θ and a limiting flux l these truncations are described by the following:

$$B_0 \geq B_{\text{iso}} / f(\zeta), \quad r_0 \geq d_A \theta / \zeta, \quad \text{and} \quad L \geq 4\pi d_L^2 l F(\infty) / F(\zeta), \quad (27)$$

where $\eta(\zeta) = \eta_0$ and $\zeta = r_p / r_0$.

Note that in contrast to the complicated truncations we found for the isophotal case, equations (10), (12) and (13), the current truncations are much simpler; they depend only

on one observational limit and the redshift. The above limits are good for $\theta \gg \theta_s$, the size of the PSF. This will always be true in this case because of the need to have a well defined surface brightness distribution.

If the truncation limits are chosen so that $l = \pi\theta^2 b_{\text{iso}}$, then the last limit in equation (27) due to the flux limitation falls below the other two and can be ignored. In this case the data truncation in the $B_0 - r_0$ plane is parallel to the axis making the calculation of the observables straight forward and free of the complex limits of integration. Since the flux limit l does not enter in the determination of the observed distribution of the sources, such a sample will not be appropriate data for tests based on source counts as a function of the flux l . But such a sample can be used to obtain the distributions of the angular size, average surface brightness or redshift. For example the latter is simply

$$N(\zeta, z) = \frac{dV}{dz} \int_{B_{\text{iso}}/f(\zeta)}^{\infty} dB_0 \int_{\theta d_A/\zeta}^{\infty} dr_0 \psi(B_0, r_0, z). \quad (28)$$

Because of this simplification, such samples are well suited for tests based on the moments of the observed distributions. For example the angular size-redshift relation is simply given as

$$\langle \pi\theta^2(z) \rangle = \frac{\zeta}{N(\zeta, z)d_A^2} \frac{dV}{dz} \int_{B_{\text{iso}}/f(\zeta)}^{\infty} dB_0 \int_{\theta d_A/\zeta}^{\infty} dr_0 \pi r_0^2 \psi(B_0, r_0, z). \quad (29)$$

Similarly, for the flux-redshift relation we have

$$\langle l(z) \rangle = \frac{F(\zeta)}{N(\zeta, z)d_L^2} \frac{dV}{dz} \int_{B_{\text{iso}}/f(\zeta)}^{\infty} dB_0 B_0 \int_{\theta d_A/\zeta}^{\infty} dr_0 \pi r_0^2 \psi(B_0, r_0, z), \quad (30)$$

or, in terms of the luminosity L

$$\langle l(z) \rangle = \frac{F(\zeta)/F(\infty)}{N(\zeta, z)d_L^2} \frac{dV}{dz} \int_{B_{\text{iso}}/f(\zeta)}^{\infty} dB_0 \int_{L_{\min, \zeta}}^{\infty} dLL \bar{\psi}(B_0, L, z), \quad (31)$$

with a similar expression for the size- z relation. The integration limit

$$L_{\min, \zeta} = 4\pi d_L^2 (\pi\theta^2 b_{\text{iso}}) (F(\infty)/\zeta^2) (B_0/B_{\text{iso}}). \quad (32)$$

These expressions are considerably simpler than the corresponding equations for the isophotal analysis.

Similar expressions can be derived for other definitions of the metric quantities. For example, as mentioned in §1 in connection with Figures 1 and 2, instead of r_p one can use the effective radius r_{eff} , within which resides a certain fraction (usually half) of the total light. This would amount to a new definition of the constant ζ as $F(\zeta) = F(\infty)/2$. This may be a convenient procedure for nearby galaxies but not at high redshifts, because it relies on the knowledge of the total flux, the determination of which lies at the heart of the difficulty associated with these tests. The procedure proposed in P76 relies only on the data within a specified radius and not on the data from the outer, invisible parts; θ_p is obtained by setting the ratio of the average to limiting surface brightnesses to a fixed value.

4. NEW TESTS

The discussions in the above two sections demonstrate that an accurate analysis of the extragalactic data for the purpose of cosmological tests is complicated and must include all of the above mentioned considerations. In particular, it is imperative to keep in mind the multivariate nature of the problem and to account for the surface brightness limitation, (eq. [7]), common in all of the above expressions. The dispersions in the distributions of B_0 , r_0 or L , and the correlations between these can have substantial effect on the final results. These effects are more pronounced when dealing with the isophotal quantities than with the metric ones. However, the latter procedure must be limited to well resolved sources, while the former, in principle, could be extended to unresolved sources if a good knowledge of the PSF is at hand.

This task, however complicated, can be carried out given the knowledge of the distribution function and the brightness profile. With sufficient care in the analysis of the

data and in modeling one can determine either the cosmological evolution of the sources (i.e. the redshift variation of the distribution ψ) or the cosmological parameters. Such analyses, which may be simple or appropriate for data limited to low redshifts is not the simplest method to determine the cosmological or galactic evolutions. For example, the traditional method of identifying sources with some apparent flux may not be necessary or be the most straight forward way of carrying out this task. The complexities described in the previous sections are the result of the multiple selection criteria needed for counting individual galaxies.

We now describe two new and much simpler tests which combine the good aspects and avoid the complexities of the two methods described above, and are much better suited for the analysis of modern digitized CCD data. The essence of these tests is to reduce the selection criteria to one, namely the surface brightness, and deal with the distribution of B_0 . In practice this amounts to simply counting the number of pixels at a given surface brightness (or adding up their intensities) independent of which galaxy they belong to. This way one can avoid the complexities arising from the need to define the sizes and fluxes (isophotal or metric) for every galaxy in the field.

4.1. Sky Covered By Galaxies

The first of these tests, which is related to the angular diameter test, involves computation of the fraction of the sky which is covered by all galaxies above (cumulative) or within (differential) a given range of surface brightness, b to $b + db$. Observational determination of this fraction is simple. It is accomplished by counting the number of pixels with a given intensity value. The expressions relating this quantity to the cosmological models and to the properties of the galaxies are decidedly (somewhat) simpler than those for the isophotal (metric) treatment. Let us first consider well resolved sources, namely

those with angular radii $\geq \theta$ which we take to be $\gg \theta_s$. In this case the only data truncation arises from the size limit which is same as that described by equations (11) and (12) with the isophotal quantities replaced by those for an arbitrary value of b .

$$B_z = (1+z)^4 b, \quad x_b \equiv \theta_b d_A / r_0 = f^{-1}(B_z / B_0) \quad \text{with} \quad B_0 \geq B_z / f(\theta d_A / r_0). \quad (33)$$

Now following the same steps as in the previous sections the sky fraction covered by all galaxies down to a given apparent surface brightness b is obtained by adding the contribution $\pi\theta_b^2 = \pi(x_b r_0 / d_A)^2$ of each galaxy. The result is

$$\mathcal{F}_{\text{sky}}(> b, z) = \frac{d\chi}{dz} \int_{B_z}^{\infty} dB_0 x_b^2 \int_{\theta d_A / x_b}^{\infty} dr_0 \pi r_0^2 \psi(B_0, r_0, z), \quad (34)$$

where the line element

$$d\chi/dz = (dV/dz)(4\pi d_A^2)^{-1}. \quad (35)$$

Alternatively, in terms of the luminosity distribution

$$\mathcal{F}_{\text{sky}}(> b, z) = \frac{d\chi}{dz} \int_{B_z}^{\infty} dB_0 \frac{x_b^2}{B_0 F(\infty)} \int_{L_{\min,b}}^{\infty} dL L \bar{\psi}(B_0, L, z), \quad (36)$$

where

$$L_{\min,b} = 4\pi d_L^2 (\pi\theta_b^2 b) F(\infty) / (x_b^2 f(x_b)). \quad (37)$$

Note that these equations have the simplicity of the tests based on metric values; equation (34), except for the term x_b^2 is identical to $(< \pi\theta^2(z) >)N(\zeta, z)$, shown in equation (29). However, more importantly, the data analysis is enormously simpler because it does not require determination of the surface brightness profile and the metric or isophotal values for each galaxy.

As in the case of the classical tests, this test also can be carried out for unresolved sources. But this is not much different than counting sources because all unresolved sources have essentially the same area, $\pi\theta_s^2$. Following the procedure in §2.3 it can be shown that the sole truncation due to the surface brightness limit, $B_0 \xi \geq B_z$, is equivalent to

$$L = 4\pi d_A^2 (\pi\theta_s^2 B_0) \xi \geq L_b \equiv 4\pi d_L^2 (\pi\theta_s^2 b) \quad (38)$$

and the actual angular radius of each source is given as $\theta_b/\theta_s = g^{-1}(B_z/B_0\xi) = g^{-1}(L_b/L)$.

Thus, the fraction of the sky covered by unresolved sources then becomes

$$\mathcal{F}_{\text{sky}}(>b, z) = \frac{dV}{dz}(\pi\theta_s^2) \int_{B_z}^{\infty} dB_0 \int_{L_b}^{\infty} dL \left(g^{-1}(L_b/L)\right)^2 \bar{\psi}(B_0, L, z). \quad (39)$$

Similarly, as in §2.4, if we have a good knowledge of the form of the PSF we can combine resolved and unresolved sources by expressing the above relations in terms of the modified profile \hat{f} as the convolution of the profile f and the PSF g [eq. (8)]. Then we do not need not to specify a size limit and the only truncation comes from the value of the apparent surface brightness b . However, in this case we have the added complication due to the dependence of the characteristics on the ratio $\theta_s d_A/r_0$. For example, equation (36) now becomes

$$\mathcal{F}_{\text{sky}}(>b, z) = \frac{d\chi}{dz} \int_{B_z}^{\infty} \frac{dB_0}{B_0 F(\infty)} \int_{\hat{L}_{\min,b}}^{\infty} dL L x_b^2 \bar{\psi}(B_0, r_0, z), \quad (40)$$

where now $\hat{L}_{\min,b}$ is given in equation (37) with $f \rightarrow \hat{f}$, $F \rightarrow \hat{F}$ and $x_b = \theta_b d_A/r_0$ is a function of both B_0 and L (or r_0) and is obtained from the inversion of the relation $\hat{f}(x_b, \theta_s d_A/r_0) = B_z/B_0\xi$, with $\pi r_0^2 = L/(B_0 F(\infty))$.

The differential distribution can be obtained from $f_{\text{sky}}(b, z) = -\partial \mathcal{F}_{\text{sky}}(>b, z)/\partial b$. The integration of either distribution over z gives the differential or cumulative distributions of all galaxies irrespective of their redshift.

4.2. Total Sky Brightness

The second test, which is related to the flux-redshift test, deals with the contribution of all galaxies to the sky brightness within a range of (or above) a given surface brightness b . This amounts to adding all of the intensity values of the appropriate pixels. This is to be then compared with the expression for the total intensity (flux per steradian) as the sum

of the contribution $l(\theta_b) = \pi r_0^2 B_0 F(x_b)/(4\pi d_L^2)$ of all resolved galaxies with $\theta_b \geq \theta$.

$$\mathcal{I}_{\text{sky}}(>b, z) = \frac{1}{(1+z)^4} \frac{d\chi}{dz} \int_{B_z}^{\infty} dB_0 \frac{F(x_b)}{F(\infty)} \int_{L_{\min,b}}^{\infty} dLL \bar{\psi}(B_0, L, z). \quad (41)$$

Note again the similarity of this expression to equation (31). As above, if we redefine the profile as the convolved \hat{f} and include all resolved and unresolved galaxies in the analysis, we obtain the relation:

$$\mathcal{I}_{\text{sky}}(>b, z) = \frac{1}{(1+z)^4} \frac{d\chi}{dz} \int_{B_z}^{\infty} dB_0 \int_{\hat{L}_{\min,b}}^{\infty} dLL \frac{F(\hat{x}_b)}{F(\infty)} \bar{\psi}(B_0, L, z). \quad (42)$$

The differential distribution is obtained as $i_{\text{sky}}(b, z) = -\partial \mathcal{I}_{\text{sky}}(>b, z)/\partial b$, and the integrals of these over z give the cumulative and differential total sky brightness as a function of b . Note that $i_{\text{sky}}(b, z) = bf_{\text{sky}}(b, z)$.

4.3. Average Sky Brightness

The ratio of the quantities described in above two tests gives the average surface brightness at or down to some surface brightness b . This quantity as expected is independent of the cosmological model parameters and depends only on the surface brightness profile and redshift and consequently, as already pointed out in P76, can be used to determine the evolution of the surface brightness. In general, this relation is more complicated than envisioned in P76 where the discussion was aimed at the brightest cluster galaxies. For a larger and varied sample of sources this relation is more complex and not as obvious. If, for purpose of illustration, we assume that B_0 and r_0 or L are not correlated, then from equation (40) and its counterpart for \mathcal{I} , this ratio becomes

$$\langle b(z, b) \rangle = b \left(\int_{B_z}^{\infty} F(x_b) h(B_0) dB_0 / \int_{B_z}^{\infty} x_b^2 f(x_b) h(B_0) dB_0 \right), \quad (43)$$

where $h(B_0)$ describes the distribution of the central surface brightness. Note that for a delta function, or a relatively narrow distribution, the above expression simplifies to

$\langle b \rangle / b = \eta(x_b)$ as is the case with individual galaxies. This demonstrates that the surface brightness profile, or the function η based on it, plays a central role in cosmological studies of extended sources.

With minor modification the above expressions will be valid for elliptical sources with constant ellipticity. For such sources with major and minor core radii r_1 and r_2 , the area within any isophotal limit is proportional to $\pi r_1 r_2$, so that if we define $r_0 = (r_1 r_2)^{1/2}$ the above expressions would apply, but we now have the additional integration over the possible dispersion of the ellipticities or the ratio r_1/r_2 .

5. SUMMARY

In this paper we deal with the analysis of the distribution of redshift-size-flux (or magnitude) data on extragalactic sources, in particular galaxies, which is often used for testing the evolution of sources and/or the universe. The usual practice is to describe the characteristics and evolution of the galaxies in terms of a simple luminosity function $\phi(L, z)$, as if the galaxies are point sources and the data is simply flux or magnitude limited. We emphasize that in reality these tests are more complicated. The proper analysis must involve the variation of the surface brightness profile and the multidimensional distribution function of the parameters that describe this profile, such as core radius, central surface brightness, luminosity, etc.; $\psi(B_0, r_0, L, \alpha, \dots, z)$. Neglecting these complexities and the truncations of the data produced by the surface brightness and angular size limits can lead to grossly misleading results.

There are different ways one can account for these effects. The most efficient use of the observations comes from comparison of the full set of the data with model predictions which include the effects of all biases that are encountered in the observational selection processes. Use of the isophotal values down to lowest possible isophot and size is a good

example of this approach. We have described the correct analysis of such a data in terms of the multivariate luminosity function ψ . We derive the relevant expressions, in terms of the surface brightness profile of spherical sources, which is to be compared with observations of the isophotal values of the fluxes, sizes and surface brightnesses. In general, because more than just the usual flux (or magnitude) limit enters in the analysis these expressions are relatively complex. Truncation of the data due to other selection effects such as angular extent and surface brightness thresholds come in and can play the dominant role in defining the content of a sample of sources. The surface brightness profile of the galaxies plays a pivotal role in these calculations.

A second approach would be to select a subset of the data which yields to a more straight forward comparison with models. For example, if we select the more limited sample of large and well resolved sources, we can use fluxes and sizes related to a metric (instead of isophotal) radius, such as the radius defined in P76 for a constant value of the η function. We derive the relevant expressions for this case and show that they are much simpler than the isophotal ones, and resemble more closely the simple expressions for point sources. This method, therefore, would be more appropriate for evaluation of the moments of the observed distributions in tests like the redshift-flux or angular size-redshift tests. The isophotal method is more appropriate approach for tests based on source counts and, in principle, can be used for samples of sources which include resolved as well as unresolved sources. With the knowledge of the PSF at hand one can use a modified surface brightness profile as convolution of the actual profile and the PSF.

The above tests, aside from the complications in the modeling, suffer from the additional shortcoming of needing elaborate procedures for the analysis of the data. To overcome some of the difficulties in both of these areas we propose a new method for the analysis and modeling of extended extragalactic sources for the purpose of determining either their evolution or the cosmological parameters. This method is very well suited to modern

digitized data, and amounts to counting the numbers of pixels or summing their intensity values. It is capable of using all the data as in the isophotal case but the expressions relating the data to models are considerably simpler and are similar to the metric ones. Their simplicity stems from the fact that they deal with the surface brightness limit alone and do not include selection based on fluxes or sizes. As already shown in P76, tests based on surface brightness tend to be more robust and simpler.

To reiterate, these new methods clearly have the following advantages.

- a) The data analysis is obviously considerably simpler.
- b) The expressions relating the observations to the distributions of the basic properties of galaxies is evidently simpler: Compare, e.g. equations (14) and (40).
- c) The dependence on the cosmological parameters is also considerably more straightforward: Instead of the dependence on the volume $V(z)$, and on the luminosity and angular diameter distances, d_L and d_A , the new tests depend primarily on the redshift and the much simpler line element $d\chi/dz$. For example, for models with zero cosmological constant this is equal to $(c/H_0)(1+z)(\Omega z + 1)^{-1/2}$, where Ω is the density parameter and H_0 is the Hubble constant.
- d) Because we are dealing with surface brightness, to first order the resulting expressions are independent of the weak gravitational lensing effects due to the inhomogeneities of the intervening matter distribution (clumpiness due to galaxies and clusters).

As mentioned above the modern digitized CCD data are ideally suited for the task proposed here. However, several conditions are required for the proper application of all the tests proposed here. A good knowledge of the background sky brightness due to all other sources except extragalactic sources underconsideration is needed because we wish to go to as low a surface brightness as possible. Application of the new methods to integrated (over

the redshift) values of \mathcal{F}_{sky} and \mathcal{I}_{sky} to the whole data say, in a CCD frame, will require accurate flat fielding. However, for redshift dependent type analysis the requirements are similar to galaxy based analysis, because redshifts are known for galaxies as a whole and not for individual pixels. For this kind of studies some identification of the pixels with galaxies is necessary so that we can assign redshifts to pixels. Secondly, when combining resolved and unresolved galaxies it is important that contaminations due to other unresolved sources such as stars is kept to an acceptable value. And Finally, in all these tests one must deal with several profiles; disks, spheroids and possibly a continuum of superposition of both. In future works we hope to use these new methods on the data from the Hubble Deep Field (see Williams et al., 1996) as well as those from ground based observations.

This work was carried out while I spent a three month sabbatical leave at the Space Telescope Science Institute. I would like to thank the director Robert Williams and the Staff of the Institute for their support and hospitality. I also would like to thank Drs. H. Ferguson, M. Vogeley and M. Fall for valuable discussions on the general topic of this paper.

REFERENCES

Impey, C. & Bothun, G. 1997, The An. Rev. Ast. & Ap., 35, —

de Jong, R. S. 1996, Adstr. & Ap., in press

Efstathiou, G., Ellis, R. S. Peterson, B. A. 1988, M.N.R.A.S ,232 431

Fish,R. A. 1964, ApJ, 139, 284

Freeman, K. C. 1970, ApJ, 160,811

Gunn,J. E., & Oke, J. B. 1975, ApJ, 195, 255

Lin, H, et al. 1996, ApJ, 464, 60

McGaugh, S. S. 1996, M.N.R.A.S. 280, 337

Metcalf, et al. 1995, M.N.R.A.S. 273, 257

Petrosian, V. 1976, ApJ(Letters), 209, L.

Sandage, A. R. 1972, ApJ, 173, 485

Sandage, Allan & Perelmutter, Jean-Marc 1991, ApJ, 370, 455

Tinsley, B. M. 1968, ApJ, 151, 547

Tinsley, B. M. & Gunn, J. E. 1976, ApJ, 203, 52

Tolman, R. C. *Relativity, Thermodynamics, and Cosmology* (Clarendon Press, Oxford, 1934)

Tully, R. B. & Verheijen, M. A. W. 1997, preprint

Tyson, T., 1988, ApJ, 96, 1

Weinberg, S. *Gravitation and Cosmology* (John Wiley, N. Y., 1972)

Williams, R. E. et al. 1996, AJ, 112, 1335

Yoshii, Yuzuru 1993, ApJ, 403, 552